Oil & Natural Gas Technology

DOE Award No.: DE-FE0010406
DUNS No.: 170230239

Quarterly Research Performance Progress Report (Period ending 9/30/2014)

CONTROLS ON METHANE EXPULSION DURING MELTING OF NATURAL GAS HYDRATE SYSTEMS: TOPIC AREA 2

Project Period (9/30/2013 to 9/30/2014)

Submitted by:
Peter B. Flemings

Peter B Flemings
Signature

The University of Texas at Austin
101 East 27th Street, Suite 4.300
Austin, TX 78712-1500
e-mail: pflemings@jsg.utexas.edu
Phone number: 512-475-9520

Prepared for:
United States Department of Energy
National Energy Technology Laboratory

November 14, 2014

Office of Fossil Energy

1 ACCOMPLISHMENTS:

1.1 What are the major goals of the project?

The project goal is to predict, given characteristic climate-induced temperature change scenarios, the conditions under which gas will be expelled from existing accumulations of gas hydrate into the shallow ocean or directly to the atmosphere. When those conditions are met, the fraction of the gas accumulation that escapes and the rate of escape shall be quantified. The predictions shall be applicable in Arctic regions and in gas hydrate systems at the up dip limit of the stability zone on continental margins. The behavior shall be explored in response to two warming scenarios: longer term change due to sea level rise (e.g. 20 thousand years) and shorter term due to atmospheric warming by anthropogenic forcing (decadal time scale).

Milestone Description	Planned Completion	Actual Completion	Verification Method	Comments (progress toward achieving milestone, explanation of deviation from plan, etc.)
1.A 1-D simulation of gas hydrate dissociation in natural systems.	9/30/2013	9/30/2013	Report	Complete
1.B 1-D Simulation of gas hydrate dissociation in laboratory controlled conditions.	3/31/2014	11/1/2013	Report	Complete
1.C Model-based determination of conditions required for gas not to reach seafloor/atmosphere from dissociating hydrate accumulation.	3/31/2014	3/31/2014	Quarterly Report	Complete
1.D Determination of what hydrate reservoirs are at three-phase equilibrium.	12/31/2013	12/1/2013	Report	Complete
1.E Demonstrate ability to create and dissociate methane hydrate within sediment columns under conditions analogous to natural systems.	9/30/2013	10/15/2013	Report	Complete
2.A 1-D simulation of gas expulsion into hydrate stability zone.	9/29/2014	9/29/2014	Report	Complete
2.B Determination of conditions for which gas expulsion into hydrate-stability zone is self-limiting.	12/29/2014	9/29/2014	This Quarterly Report	Complete
2.C Demonstration of reaction transport experiment where gas invades hydrate stability zone and creates three phase stability.	9/30/2014	9/29/2014	This Quarterly Report	Currently developing/refining remote sensing technologies. Refining experimental design based on numerical simulation
2.D Demonstrate a 2D simulation of hydrate dissociation and gas expulsion.	3/31/2015		Report	

1.2 What was accomplished under these goals?

1.21 PHASE 1/BUDGET PERIOD 1

Task	Projected Finish	Actual Finish	Summary
Task 1: Project Management and Planning	9/30/15	In process	Monitoring & controlling project
Task 2: Conceptual and Numerical Model Development -1D	3/31/14	3/31/14	Task 2 has been completed.
Task 3: Categorize stability of known hydrate reservoirs	9/30/13	9/30/13	Task 3 has been completed.
Task 4: Laboratory Evaluation of Hydrate Dissociation	3/31/14	6/1/14	Task 4 has been completed.

1.22 PHASE 2/BUDGET PERIOD 2

Task 5: Gas expulsion modeling
Projected Finish: 9/28/15
Actual Finish: in process

Subtask 5.1 - Develop 1D model of gas expulsion into water-saturated hydrate-stability zone
Projected Finish: 9/29/14
Actual Finish: 9/29/14
This model is fully developed.

Subtask 5.2 - Apply 1D expulsion to laboratory experiments
Projected Finish: 3/30/15
Actual Finish: 9/29/14
The model has been developed and presented in the June 2014 report.

Subtask 5.3 - Apply 1D model to natural hydrate accumulations
Projected Finish: 9/28/15
Actual Finish: in process
The model is currently being applied to the permafrost zone such as in Alaska (Figures 1-4) and to the deepwater continental margins (Figure 5).

Permafrost Zones:
We consider an initial condition similar to those at the Malik Well (Dallimore and Collett, 2005). Malik gas hydrate field is located in Mackenzie delta on the coast of Beaufort Sea, in the northwest territories of Canada (Dallimore and Collett, 2005). It was shown to be one of the most concentrated gas hydrate deposits in the world (Dallimore and Collett, 2005). Relatively thick sections of high-saturation methane

hydrate (often over 80%) lie between 897 and 1110 m (Taylor et al., 2005). Ice-bearing permafrost extends from ground surface to the depth of about 600m (Henninges et al., 2005).

In our simulation, the initial water pressure increases hydrostatically with depth (Fig. 1a). Present average ground surface temperature is -6^{o}C (Majorowicz et al., 2012) (Fig. 1b). We set the initial temperature at the base of the permafrost (BP) (600 m) at -1^{o}C (Henninges et al., 2005) (Fig. 1b). Below that temperature increases linearly with the gradient of 26^{o}C km-1 (Fig. 1b) (Henninges et al., 2005). A fixed geothermal flux of 56 mW m^{-2} is applied at the lower boundary (1400 m), providing an equilibrium initial temperature distribution. Sediments in the shallow depth of the Beaufort-Mackenzie Basin is largely terrestrial, and low salinities below 0.1-0.5 wt.% can be expected (Dallimore and Collett, 2005). We set the BP at 600 m. We assume the salinity from ground surface to 600 m to be 0.5 wt.% before ice formation (denoted as X^s_{l0}). After ice formation, the initial brine in the permafrost has a salinity equilibrating with the ice phase (denoted as X^s_{l+i}), which is calculated according to the phase curve of ice and water and decreases linearly downward (Fig. 1d). We assume there is no salt transport during ice freezing. The initial ice saturation (S_i) can be calculated from the mass conservation of salt as $S_i = 1 - \frac{X^s_{l0}}{X^s_{l+i}}$ (Fig. 1c). We call this case as High Ice Saturation. The initial salinity under the permafrost is uniformly 3 wt.% (Fig. 1d). This puts the BHSZ at 1100 m. Two hydrate layers with variable saturations exist from 900 to 1000 m, and from 1080 to 1100 m (Fig. 1c). The initial hydrate saturations are obtained by averaging the nuclear magnetic resonance-derived gas hydrate saturation for Malik 5L-38 well (Dallimore and Collett, 2005). The porosity is uniformly 35%, and the permeability of the gas-hydrate-free sediments is 10^{-13} m^2 (Dallimore and Collett, 2005).

At time zero we increase the ground surface temperature linearly from -6 to 0^{o}C over300 years and then keep the surface temperature at 0^{o}C for the remaining time. This temperature forcing is to reflect future climate warming caused by doubling of CO_2 in the atmosphere (Majorowicz et al., 2012). Ice melts from ground surface immediately as the temperature there is increased because the system thermodynamic status is initially on ice-brine phase boundary (Fig. 2a, b). Ice also melts from the BP (Fig. 2b), which is caused by the geothermal flux (Archer et al., 2009). Ice front retreats faster from the BP (Fig. 2b). There are two reasons for this: first, the initial ice saturation decreases with depth and reaches minimum at the BP; second, there is a large initial salinity gradient toward the BP, and salt diffusion toward the BP promotes ice melting there. At 30 k.y. the ice layer has shrunk to the depth between 40 and 140 m with an average saturation of 20% (Fig. 2b). Ice disappears at 32 k.y..

Hydrate dissociation initiates from the base of the hydrate stability zone (BHSZ). Hydrate dissociation provides methane to the shallower hydrate layer, where secondary hydrate forms (Fig. 2b). This increases the local salinity, brings the system to three-phase (hydrate, liquid and gas) equilibrium and creates a gas passage through the hydrate layer (Fig. 2a, b). As the BHSZ rises, more methane is provided to the shallower depth, and the entire hydrate deposit moves upward (Fig. 2b). Hydrate dissociation rate is very slow during the first 30 k.y., when considerable amount of ice still exists. For example, at 15 k.y., negligible amount of hydrate dissociates at its initial base (Fig. 2b). At 30 k.y., some hydrate still lies in the deeper hydrate layer, and large amount of secondary hydrate forms in the shallower hydrate layer (Fig. 2b). However, after ice disappears at 32 k.y., temperature increases and the remaining hydrate dissociates rapidly. Methane gas starts venting to atmosphere at 38 k.y., when the entire ice layer has already disappeared and the hydrate layer has risen to 540 to 980 m. Hydrate layer continues rising with methane gas venting at ground surface. The entire hydrate layer disappears at 65 k.y.. At 80 k.y. a new steady-state temperature field is built, which increases linearly with depth from 0^{o}C at ground surface with a gradient of 17^{o}C/km (Fig. 2a). Residual gas saturation (2%) remains in the sediment. Ice

and hydrate melting redistributes salinity in the sediment (Fig. 2c). Salinity in the original ice layer is much lower than the initial value (Fig. 2c). Salinity in the original hydrate layers reduces to about one third of the initial value (Fig. 2c).

Another two cases were run: Low Ice Saturation and No Ice. We decrease the initial ice saturation at each depth to one half of that in the above case ($S_i = \frac{1}{2}\left(1 - \frac{X^s_{l0}}{X^s_{l+i}}\right)$) and denote this case as Low Ice Saturation. We set the initial ice saturation in the entire subsurface to be zero and denote this case as No Ice. Similar behaviors as those in High Ice Saturation are observed except that the time for methane gas starting venting at ground surface and for the entire hydrate deposits disappearing decreases substantially (Figs . 3 and 4). In Low Ice Saturation case, methane gas starts venting at ground surface at 29 k.y., 9 k.y. earlier than High Ice Saturation case (Figs . 3 and 4). The entire hydrate layer disappears at 56 k.y., 9 k.y. earlier than High Ice Saturation case (Figs. 3 and 4). In No Ice case, methane gas reaches ground surface at 20 k.y., 18 and 9 k.y. earlier than High and Low Ice Saturation cases, respectively (Figs . 3 and 4). The entire hydrate layer disappears at 46 k.y., 19 and 10 k.y. earlier than High and Low Ice Saturation cases (Figs. 3 and 4), respectively. These differences are caused by the latent heat of ice melting, which strong buffers hydrate dissociation. The latent heat of ice melting delays and attenuates heat transport to the hydrate layers. A high ice saturation requires and retards more heat from ground surface.

The methane gas venting rate at ground surface fluctuates with time (Fig.4). Once methane gas starts venting at ground surface, the methane flux rate or the hydrate melting rate does not depend on the initial ice saturation in the subsurface (Figs. 3 and 4). There are two stages of gas venting in all the three cases: the first stage lasts about 14 k.y. with an average flux rate of 0.48 g m^{-2} yr^{-1}, and the second stage lasts about 13 k.y. with an average flux rate of about 0.30 g m^{-2} yr^{-1} (Figs. 3 and 4).

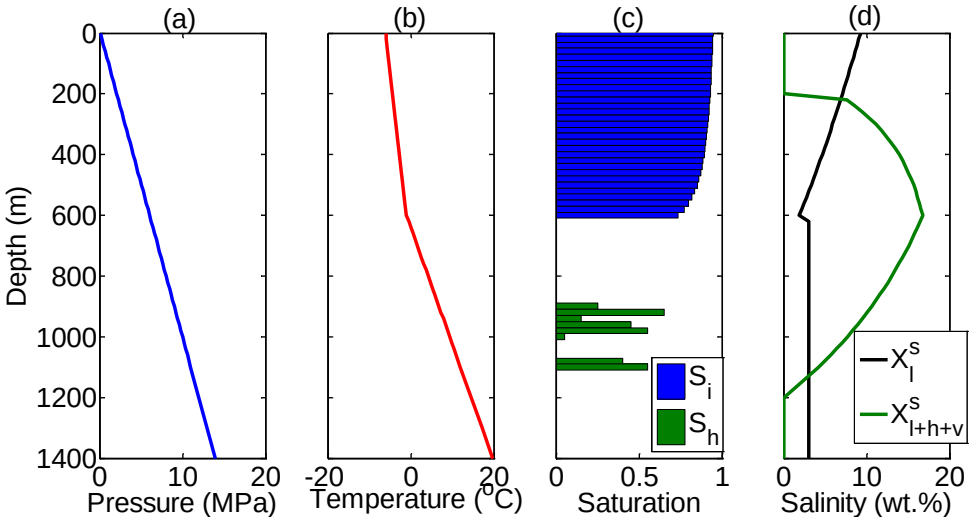

Figure 1: Initial (a) pressure, (b) temperature, (c) saturation and (d) salinity distributions for Mallik case 1. Si is ice saturation, Sh is hydrate saturation, X^s_l is initial input salinity, and X^s_{l+h+v} is three-phase equilibrium salinity for liquid, gas and hydrate phases.

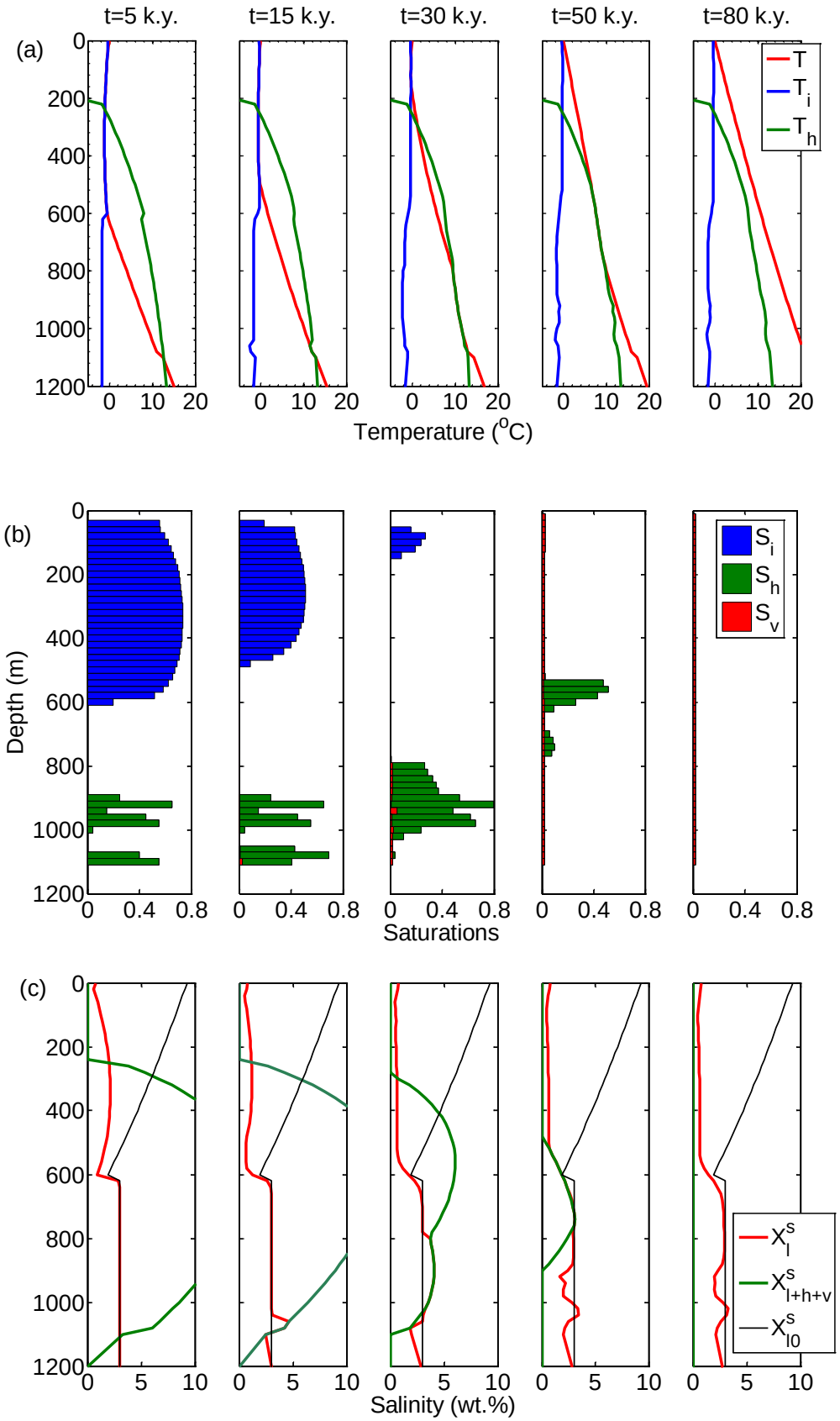

Figure 2: High ice saturation. (a) temperature (T), equilibrium temperature for ice and liquid (T_i), and three-phase equilibrium temperature for liquid, gas and hydrate (T_h), (b) ice (S_i), hydrate (S_h) and gas saturation (S_v), (c) salinity (X^s_l),

three-phase equilibrium salinity for liquid, gas and hydrate (X^s_{l+h+v}) and initial salinity (X^s_{l0}) at 5, 15, 30, 50 and 80 k.y., respectively.

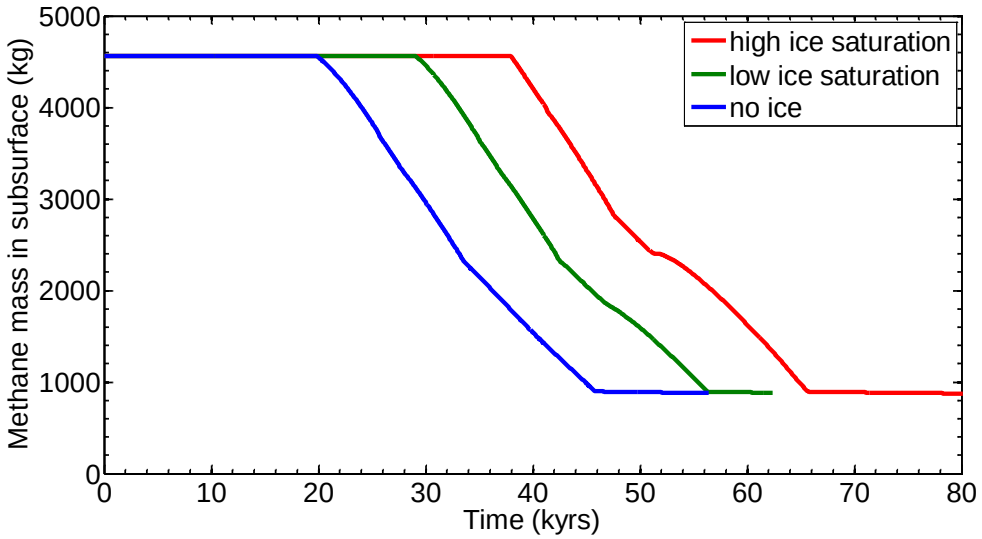

Figure 3: Evolution of total methane mass remained in subsurface when the initial ice saturation is high, low and zero.

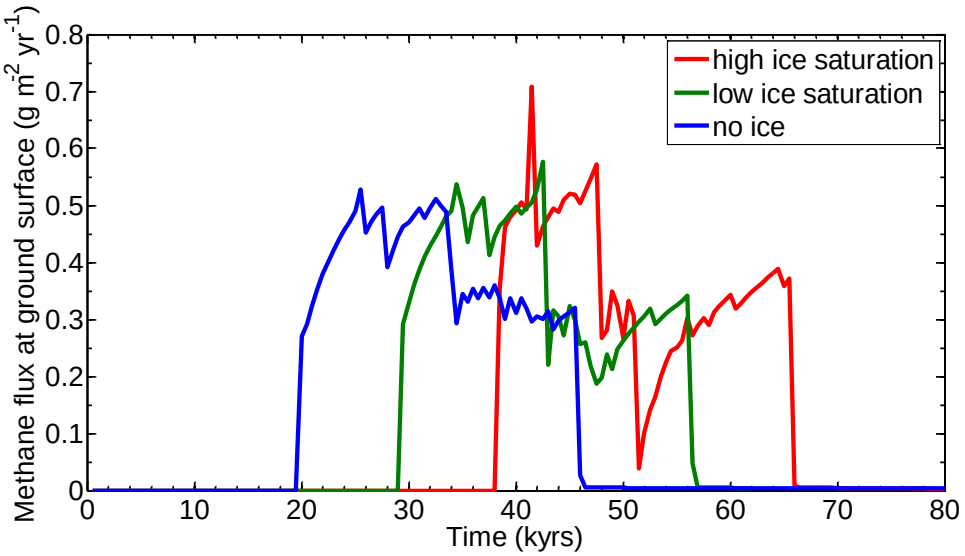

Figure 4: Evolution of methane gas flux at ground surface when the initial ice saturation is high, low and zero.

Continental Margins:

On continental margins, we have extended our numerical results to describe the general behavior of venting in hydrate systems and to specifically constrain when gas will vent due to a thermal perturbation and when it will not (Milestone 2.B). An analytical model captures the general behavior.

In the analytical model, we compare the mass of gas liberated by warming against the mass of gas that the warmed and shortened regional hydrate stability zone (RHSZ) can actually convert to hydrate. The

liberated hydrate amount determined by the initial conditions, while the allowable hydrate amount in the warmed and shortened RHSZ is set by the three-phase equilibrium conditions. If more gas is available due to warming than is allowable by the system, venting temporarily occurs.

We calculate the depth of the BRHSZ after complete warming, B_f. We assume that all hydrate beneath B_f dissociates, that no hydrate is initially above B_f, and that any salt transport is negligible[1]. We estimate the mass of gas supplied by dissociation, α, as

$$\alpha = A\rho_h \int_{B_f}^{B_i} S_h(z)dz \quad , \qquad (1)$$

where, S_h is initial hydrate saturation, ρ_h is hydrate density and A is the nominal area (1 m^2). We then calculate how much gas, γ, is necessary to establish a three-phase equilibrium chimney from B_f to the seafloor.

$$\gamma = A\rho_h \int_0^{B_f} S_h^{eq}(z)dz = A\rho_h \int_0^{B_f} \left(1 - c_0 / c_{eq}(z)\right)dz \quad , \qquad (2)$$

where S_h^{eq} is the hydrate saturation corresponding to three-phase equilibrium salinity, c_0 is the initial salinity (3.5 w.t. %), and c_{eq} is the three-phase equilibrium salinity after complete warming. Then, Λ is the ratio of gas supplied (α) to the amount of hydrate needed to form a vent (γ):

$$\Lambda = \alpha\gamma^{-1} . \qquad (3)$$

Transient venting occurs when $\Lambda > 1$ and when a RHSZ remains after warming ($B_f > 0$). *Complete venting* occurs when the RHSZ vanishes after warming ($B_f \leq 0$), as others have shown (Archer et al., 2009; Reagan and Moridis, 2009); *no venting* occurs under all other scenarios. We have compared the results of our numerical model with this analytical approach and they predict similar behavior (filled circles, Fig. 5b).

We use the analytical model to describe potential outcomes of warming for an idealized continental margin (Fig. 5a,b). For simplicity, we assume the bottom water temperature along the margin is initially constant at 3 C. We choose 3 C to coincide with the hypothesized minimum temperature of the most recent glaciation (Brothers et al., 2014). The initial RHSZ pinches-out at approximately 415 mbsl, so no hydrate can initially exist up-slope of this location (assuming an initial steady-state system). When the system is warmed by any amount, the RHSZ pinch-out moves down-slope into greater water depths. According to our model, the dissociated zone between the initial and warmed RHSZ pinch-out should produce *complete venting* of all hydrate in the sediment column. In addition, *transient venting* of hydrate will occur a finite distance down-slope of the final location of the RHSZ pinch-out. This distance is controlled by the magnitude of warming and the total hydrate initially in the system.

When the idealized system is warmed 2.5 C, the RHSZ pinch-out moves down-slope a lateral distance of 400 m to a water depth of 530 m (Fig. 5a). *Transient venting* occurs over a region of 200 m down-slope of the warming RHSZ pinch-out if hydrate initially occupied 5% of the pore space within the sediment column. The occurrence of *transient venting* for these general conditions is corroborated by dynamic simulations (black dots, Fig. 5b).

[1] Multiple simulations showed that salt transport was negligible.

These results seem to explain the observations presented by Skarke et al. (2014). They found a large set of seeps (also called vents) along the Eastern Atlantic continental margin. When the seeps are mapped using their water depths and bottom water temperatures (Fig. 5c), the seeps naturally fall into 4 seep types. Some seeps are too shallow to ever host hydrates (water depth < 300 m), while some seeps are so deep they are likely controlled by faulting and salt diapirism (Skarke et al., 2014) (water depth >1500 m). In addition, some seeps are up-slope of the modern RHSZ implying venting from increased bottom water temperature (analogous to *complete venting)*. And, finally some seeps actually appear to be within the RHSZ just down-slope of the RHSZ pinch-out. These seeps are clustered at ~550 mbsl with a bottom water temperature of 5.5 C. The combined evidence suggests this last category of seeps are examples of *transient venting* and are currently displaying gas venting from a past warming. Long-term monitoring of these seeps and/or shallow drilling would be required to further confirm these results.

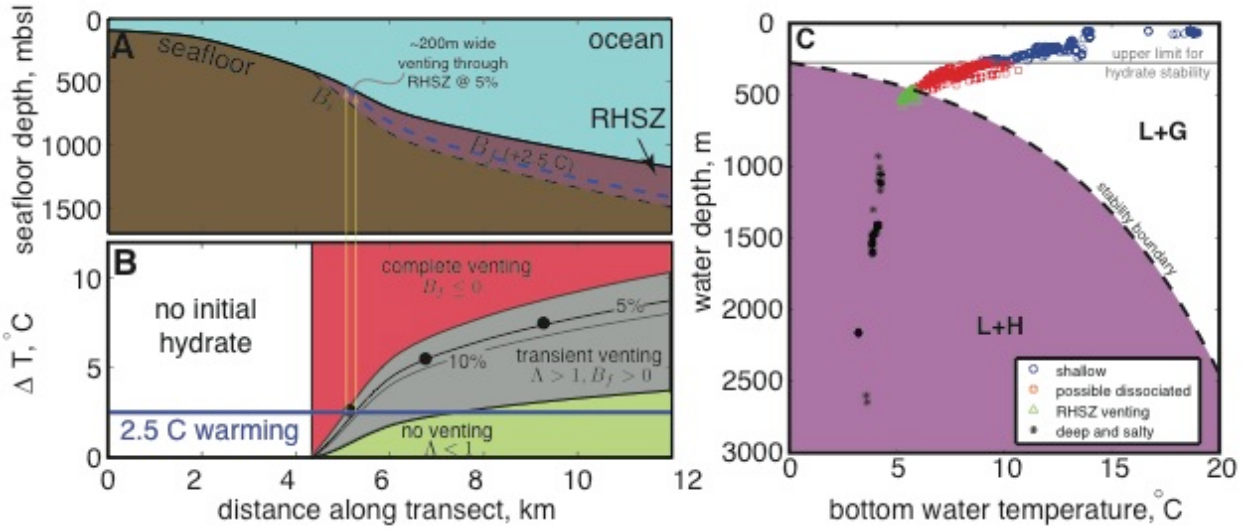

Figure 5: Warming response for an idealized continental margin using simple analytical model. (A) **Dip-section of continental margin taken from Eastern Atlantic. We mark initial BRHSZ (base of the regional hydrate stability zone), B_i , with a black dashed line and the warmed BRHSZ, B_f , with a blue dashed line. Initially, the temperature everywhere is 3 C at seafloor and increases 40 C / km.** (B) **Warming response along section where the response is *complete venting* (red region) for a large warming, *no venting* (green region) for a small warming, and *transient venting* (gray region) for warming in between the two end-member responses. *Transient venting* at a given temperature increase requires hydrate saturation greater than saturation curve within transient venting zone. Simulation results recording *transient venting* are shown with black, filled circles. Yellow arrows denote region where *transient venting* is expected for 5% hydrate saturation within the dissociated zone at the 2.5 C warming.** (C) **Plot of bottom water temperature versus water depth for the 577 seeps observed by Skarke et al. (2014). Purple region denotes where water and hydrate is stable (L+H) at the seafloor for a salinity of 3. 5 w.t. % and white region denotes where water and gas is stable (L+G). Seeps located in water depths shallower than ~300 m cannot be cooled into the hydrate stability zone.**

Task 6: Gas expulsion experiments
Projected Finish: 9/28/15
Actual Finish: in process

Subtask 6.1 - Gas invasion into water-saturated hydrate saturated zone
Projected Finish: 12/29/14
Actual Finish: in process

As reported in our previous Quarterly Report (June 2014), we have not yet successfully modeled gas invasion into the hydrate stability field. In our previous attempt, we could not get a clear gas invasion front. Over the last quarter, we have focused on generating a gas propagation front just by forcing air into water. Now that we have clearly demonstrated this behavior, we will begin over the next quarter to use methane to force gas into water-saturated sand within the hydrate stability zone.

Because of heterogeneity in our experimental system sand packs even with a uniform sand, we performed a number of "off line" experiments to refine our packing technique. These experiments included drainage in three sands under different conditions. Our sands were F110 Silica sand as in previous experiments, slightly coarser Sigma Aldrich (SA) silica sand, and even coarser but less uniform Lane Mountain #30 (LM#30) silica sand. The first two rounds of tests were performed by partially filling a container with water, constantly pouring sand into the water ("one-pour") over several minutes to reach ~ 5 inches of sand, and compaction using vibration. The third round was performed by applying constant vibration with constant "one-pour" sand emplacement. All tests were expected to test drainage under capillary-force dominated conditions. In Tests 1 and 2, water was allowed to drain through a tube attached to the bottom of the container, and then bent around until the level was about the midpoint of the sample (to form a water table in the sample, Figure 6). The surface was left open, and evaporation occurred. The third test was performed by using a syringe pump to withdraw water at the same rate we used in previous experiments, with no evaporation.

Figure 6: General test setup.

Results in Test 1, we used all three sands, and allowed the water to drain for several days. Evaporation caused the water in the drainage tube to withdraw back into the sample. Figures 7-9 show 3 cross sections of the samples, with the yellow lines in the upper left image identifying the location of the cross section cuts.

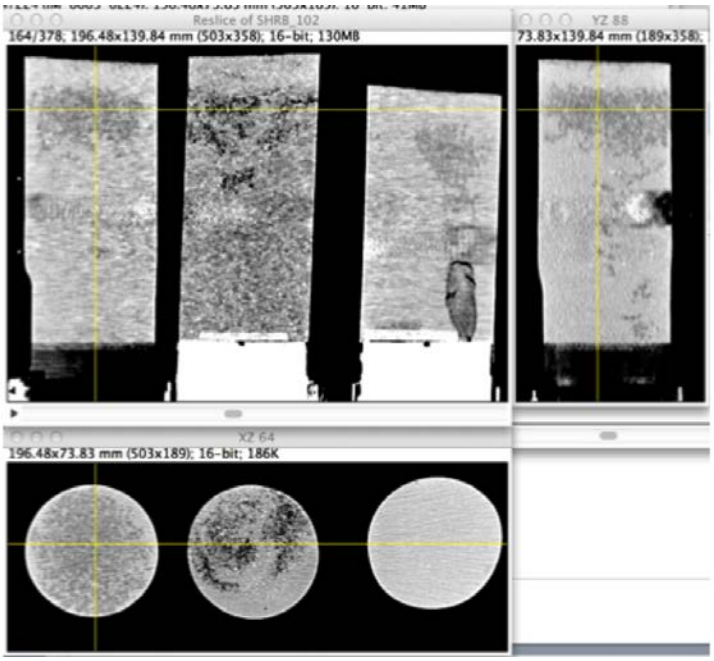

Figure 7: Water drainage from SA, LM30, and F110 sands (left to right). Upper and lower left – cross section through the three samples, Upper right, cross section through the SA sand. Drainage results in a reduction in density, here indicated by a darker color.

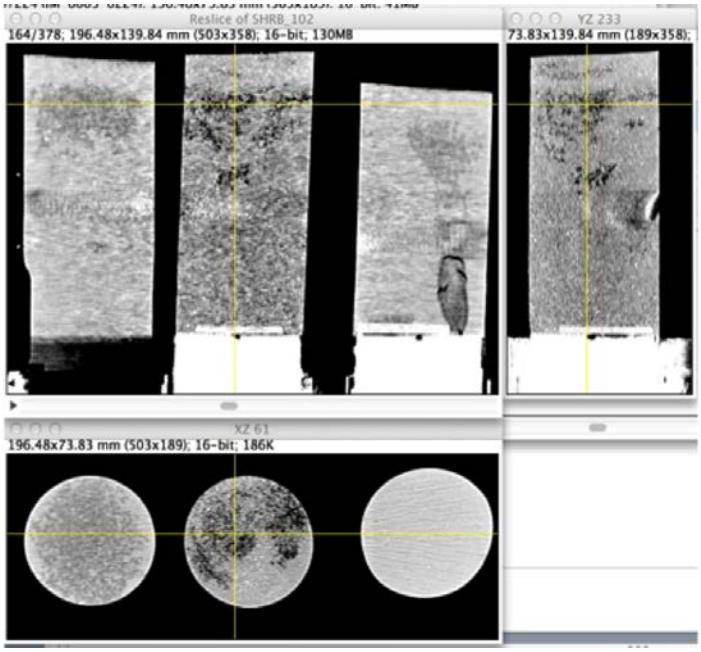

Figure 8: Water drainage from SA, LM30, and F110 sands (left to right). Upper and lower left – cross section through the three samples, Upper right, cross section through the LM30 sand. Drainage results in a reduction in density, here indicated by a darker color.

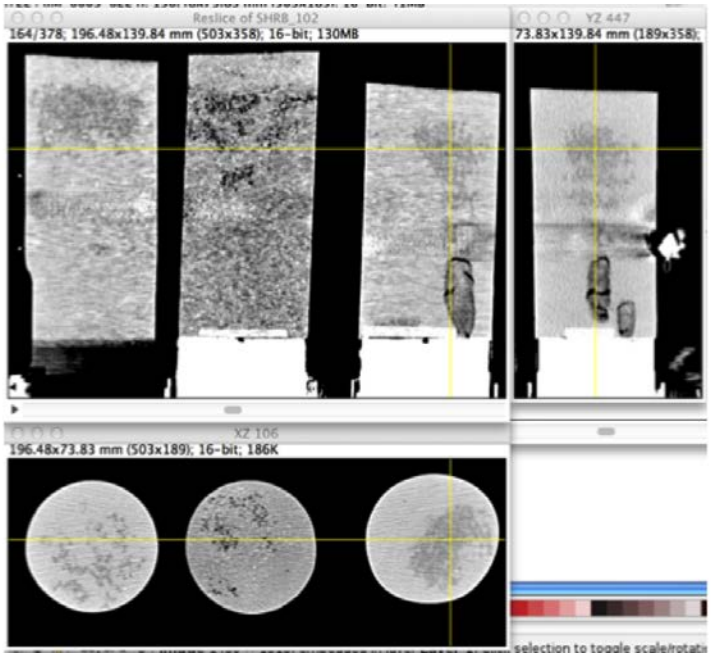

Figure 9: Water drainage from SA, LM30, and F110 sands (left to right). Upper and lower left – cross section through the three samples, Upper right, cross section through the F110 sand. Drainage results in a reduction in density, here indicated by a darker color.

The drainage in all three cases was somewhat nonuniform, with the SA sand giving the most uniform drainage. The second round of tests repeated the drainage test for the SA sand, and used a layered SA/LM30 sand combination. Figures 10 and 11 show that drainage in the SA sand was nonuniform, but

drainage in the layered sand was as expected. The water was uniformly removed from the coarse layers, but drainage was nonuniform in the fine layers.

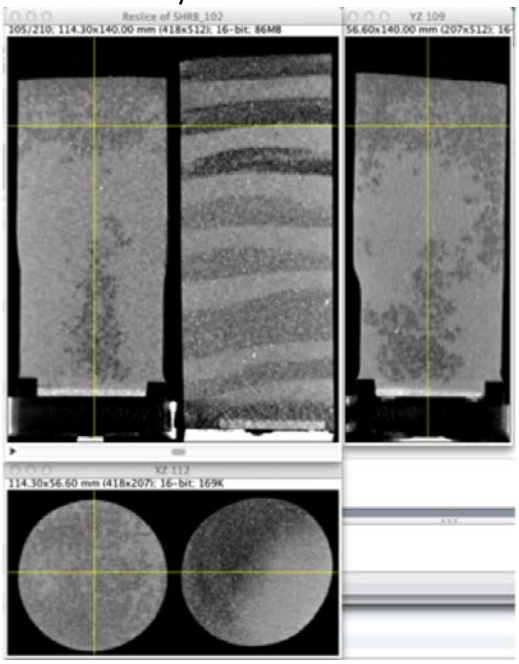

Figure 10: Water drainage from SA (left), and layered SA/LM30 sands (right) after six days. Upper and lower left – cross section through the two samples, Upper right, cross section through the SA sand. Drainage results in a reduction in density, here indicated by a darker color.

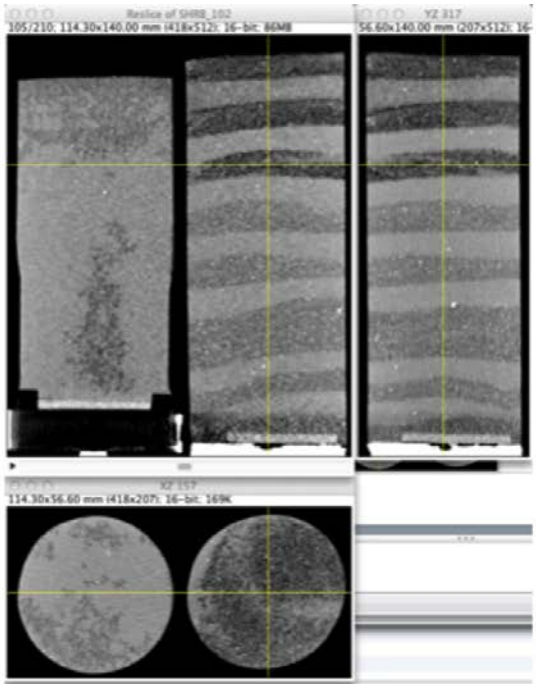

Figure 11: Water drainage from SA (left), and layered SA/LM30 sands (right) after six days. Upper and lower left – cross section through the two samples, Upper right, cross section through the layered SA/LM30 sand. Drainage results in a reduction in density, here indicated by a darker color.

The saturated SA sand is more dense than the saturated LM30 sand. The third test (Figure 12) was performed using SA sand with uniform extraction at 0.003 mL/min, and evaporation was prohibited. Although the drainage was somewhat nonuniform, the behavior was more uniform than for previous tests with the SA sand. The center of the column appears to be the most porous and easiest to drain. This is likely because the vibration energy was applied such that the column sides impacted the sample, with the center of the sample being more protected from the vibration.

The conclusions of these tests are that horizontally layered packing could potentially be used to cause a "uniform" drainage of the larger grain sized sand. Test 3 (Fig. 12) indicates that packing while vibrating the sample may affect the packing density, however the resulting packing is more suitable for our tests than the packing used in earlier tests.

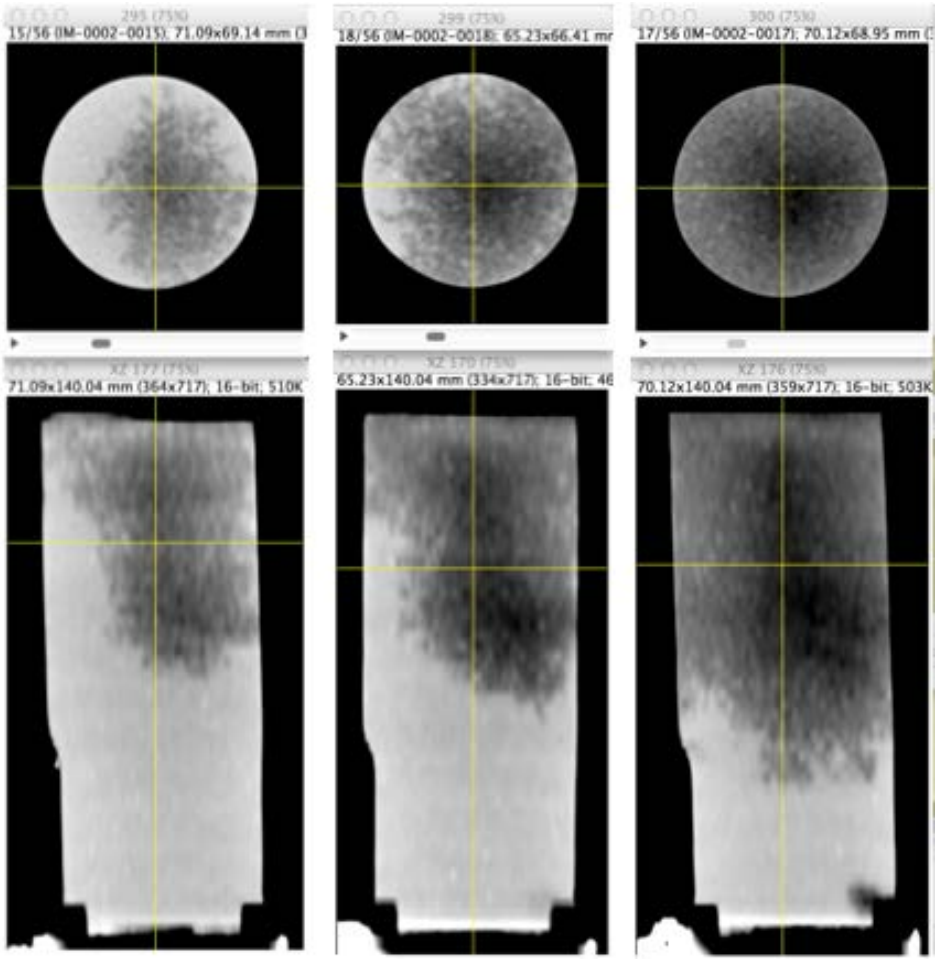

Figure 12: Water drainage from SA sands at 0.003 mL/min at 74 (left), 144 (center), and 235 (right) hours (left to right). Drainage results in a reduction in density, here indicated by a darker color.

Our experimental efforts have been more challenging than we expected. To increase our productivity in these tasks and to meet our objectives, we have manufactured an additional hydrate formation cell. This new cell (Figure 13) holds a cylindrical soil sample with the maximum dimensions of a 3" diameter and 7" length. It has been engineered to maintain a max pressure of 2500psi (~2200psi fluid pressure), which will increase the amount of subcooling we can achieve while maintaining a hydrate saturation less than 50 percent. The increased subcooling should help form hydrate faster and more consistently. This

equipment will be used at the University of Texas at Austin to perform experiments similar to those being conducted at Lawrence Berkeley National Laboratory.

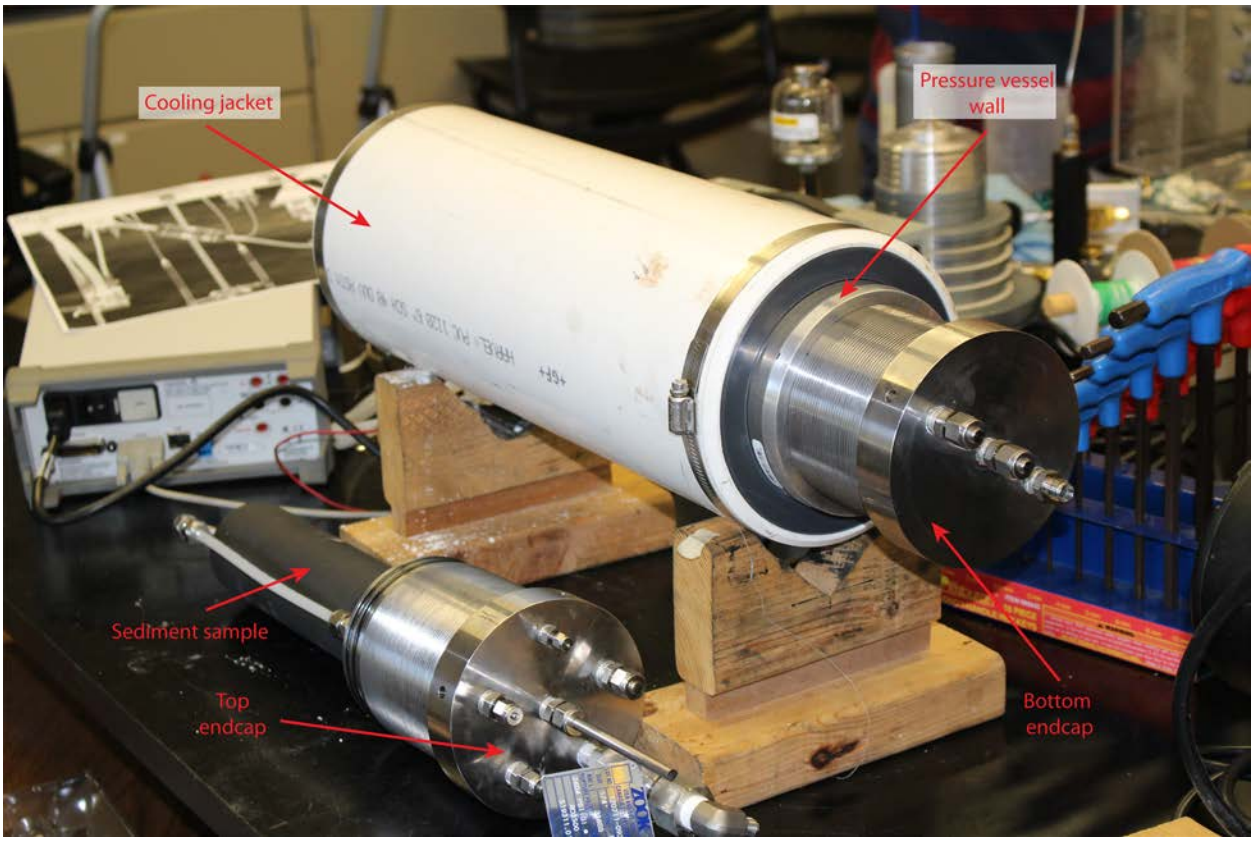

Figure 13: The UT Austin hydrate formation cell with the cooling jacket attached. There are a total of 9 fluid and instrument ports (6 on the top; 3 on the bottom) in the endcaps. Sample is confined with a fluid impermeable sleeve.

Subtask 6.2 - Gas invasion from melting hydrate into water saturated HSZ
Projected Finish: 9/28/15
Actual Finish: in process
We have not begun this task.

Task 7: 2D model
Projected Finish: 9/28/15
Actual Finish: in process
We have not begun this task.

Subtask 7.1 - Hydrate dissociation in 2D systems
Projected Finish: 9/29/14
Actual Finish: in process
We have not begun this task.

Subtask 7.2 - Gas expulsion in 2D systems
Projected Finish: 3/30/15
Actual Finish: in process
We have not begun this task.

Subtask 7.3 - Apply 2D, gas expulsion model to natural examples
Projected Finish: 9/28/15
Actual Finish: in process
We have not begun this task.

Subtask 7.3.1 Pleistocene to Holocene Sea level rise
Projected Finish: 9/28/15
Actual Finish: in process
We have not begun this task.

Subtask 7.3.2 - Recent warming
Projected Finish: 9/28/15
Actual Finish: in process
We have not begun this task.

1.3 What opportunities for training and professional development has the project provided?

There has been strong interaction between UT and LBNL over this past quarter. Our graduate students and our post-doctoral scientist are now fully working with both institutions. A particularly ripe interface is that our students and post-doc are working closely with experimental efforts at LBNL. There is continuous interaction between petroleum engineering and geosciences as we address this problem.

1.4 How have the results been disseminated to communities of interest?

Abstract and Paper Submissions

- Darnell, K., Flemings, P.B., Bryant, S.L., submitted, Transient venting of submarine arctic methane hydrate systems from moderate warming at sea floor, Geophysical Research Letters.
- Darnell, K., Flemings, P.B., 2013, Methane hydrate destabilization sensitivity to physical complexity and initial conditions in a numerical model, Abstract to be presented at *2013 Fall Meeting*, AGU, San Francisco, Calif., 9-13 Dec.
- Kneafsey, T., Flemings, P.B., Bryant, S., You, K., Polito, P., 2013, Preliminary Experimental Examination Of Controls On Methane Expulsion During Melting Of Natural Gas Hydrate Systems, Abstract to be presented at *2013 Fall Meeting, AGU*, San Francisco, Calif., 9-13 Dec.
- Meyer, D., Flemings, P.B., 2013, Thermodynamic state of hydrate-bearing sediments on continental margins around the world, Abstract to be presented at *2013 Fall Meeting, AGU*, San Francisco, Calif., 9-13 Dec.

- Meyer, D., Flemings, P.B., 2014, Thermodynamic State of Hydrate-Bearing Sediments on Continental Margins Around the World, Abstract presented at *2014 Offshore Technology Conference*, Houston, TX, 5-8 May.
- You, K., Flemings, P.B., Bryant, S., Kneafsey, T., Polito, P., 2014, Methane Hydrate Formation And Dissociation At Three-Phase Equilibrium At Constant Pressure, Abstract presented at *Gordon Research Conference: Natural Gas Hydrate Systems*, Galveston, TX, 23-28 March.
- You, K., Flemings, P.B., Bryant, S., Kneafsey, T., Polito, P., 2014, Salinity-buffered methane hydrate formation and dissociation in gas-rich systems, *Journal of Geophysical Research: Solid Earth*, submitted.

1.5 What do you plan to do during the next reporting period to accomplish the goals?

1.51 Task 5.00: Gas expulsion modeling

We will complete our write up of our 1D model to arctic systems and we will complete our write up of our approach to estimate under what conditions venting will occur.

1.52 Task 6.00: Gas expulsion experiments

We have now confirmed that we can generate a stable gas front (Fig. 12). We will focus over the next quarter on propagating a stable gas front into the hydrate solidification front.

1.53 Task 7.00: 2D model

We will begin work on this task in the coming quarter.
We will begin work on this task in the coming quarter.

2 PRODUCTS:

2.1 What has the project produced?

We have now produced a one dimensional, coupled; hydrate formation code that simulates the thermo-chemical response of a hydrate system to perturbation. We have demonstrated three-phase stability through experimental analysis and we have modeled the behavior. We have also characterized the in-situ thermodynamic state of a number of hydrate locations around the world and shown that in at least two locations, local thermodynamic conditions are altered by high salinity. We have demonstrated an approach to estimate whether or not gas venting will occur for a given thermal perturbation. We have developed a model that couples both ice and hydrate solidification/melting in response to surface temperature change.

3 PARTICIPANTS & OTHER COLLABORATING ORGANIZATIONS:

3.1 What individuals have worked on the project?

Provide the following information for: (1) principal investigator(s)/project director(s) (PIs/PDs); and (2) each person who has worked at least one person month per year on the project during the reporting

period, regardless of the source of compensation (a person month equals approximately 160 hours of effort).

Name	Peter Flemings	Steve Bryant	Tim Kneafsey	Dylan Meyer	Ebrahim Roasromani
Project Role	Principal Investigator	Co-Principal Investigator	Co-Principal Investigator	Graduate Student	Graduate Student
Nearest person month worked	.25	.25	1.25	1	1
Contribution	Advised graduate student Meyer, managed project, and recruited students. Worked with technicians for thermistor development.	Advised graduate student Meyer on analysis of models of pore space alteration due to hydrate growth and its effect on saturation exponent.	Set up experiment, ran tests, and analyzed data.	Performed analysis of thermodynamic state of 4 locations.	Performed analysis of data.
Funding Support	The University of Texas	The University of Texas	Lawrence Berkeley National Lab	JSG Fellowship	The University of Texas
Collaborated with individual in foreign country	No	No	No	No	No

Name	Peter Polito	Kris Darnell	Kehua You	Tessa Green	
Project Role	Laboratory Manager	Graduate Student	Post Doc	Project Coordinator	
Nearest person month worked	1.5	1	3	1	
Contribution	Participated in conference calls on experimental design. Ran experimental tests.	Performed literature review and theoretical calculation to prepare for laboratory experiments	Performed literature review and theoretical calculation to prepare for laboratory experiments	Coordinate meeting logistics, archive documents, and manage financials.	
Funding Support	The University of Texas	The University of Texas	The University of Texas	The University of Texas	
Collaborated with individual in foreign country	No	No	No	No	

3.2 What other organizations have been involved as partners?

Organization Name: Lawrence Berkeley National Lab

Location of Organization: Berkeley, CA
Partner's contribution to the project (identify one or more)

- In-kind support: partner makes lab space and equipment available for experiments. (e.g., partner makes software, computers, equipment, etc., available to project staff);
- Facilities: Experiments are performed in partner's lab space using equipment largely supplied by the partner (e.g., project staff use the partner's facilities for project activities);
- Collaborative research: Partner collaborates with the project staff. (e.g., partner's staff work with project staff on the project); and

3.3 Have other collaborators or contacts been involved?

No

4 IMPACT:

4.1 What is the impact on the development of the principal discipline(s) of the project?

Geological models of gas transport and hydrate melting and solidification have suggested that free gas cannot migrate through the hydrate stability zone during melting. In contrast, we suggest that free gas can migrate through the hydrate stability zone by altering the conditions of hydrate stability to a state of three-phase equilibrium through the elevation of salinity and possibly temperature. This results in fundamentally different macro-scale behavior during melting and may result in greater gas venting than has been previously demonstrated. If this hypothesis is correct, it may engender a new generation of field and laboratory investigations to document this behavior in both the field of geosciences and petroleum engineering. Second, the project links theoretical development with laboratory modeling because the concepts can be applied at the laboratory scale as well as the field scale. The laboratory experiments to be conducted will enable validation of the mechanisms incorporated in the models. These laboratory experiments will play a key role in demonstrating the processes.

4.2 What is the impact on other disciplines?

A likely outcome of our work is a more quantitative prediction of the magnitude of methane flux from the earth to the atmosphere over human (decadal) timescales and geological timescales (10,000 years). These will serve as boundary conditions for atmospheric climate models. In turn, these results may guide policy decisions.

4.3 What is the impact on the development of human resources?

We are working at the interface of geosciences and engineering. We are coupling theory and laboratory experiments to address macro-scale geologic problems. This is training a new generation of geoscientists and engineers to think with a systems-based approach that links observation with theory.

The results are being applied in the classroom and the support is training several graduate students.

4.4 What is the impact on physical, institutional, and information resources that form infrastructure?

The project is strengthening the experimental efforts and capability at UT as it is our job to develop sensor equipment. The project is strengthening development at LBNL where primary experimental work is occurring.

4.5 What is the impact on technology transfer?

We are presenting our research to approximately 100 industry members at our GeoFluids consortium (Feb 2015) and we will be presenting at a range of national and international meetings.

4.6 What is the impact on society beyond science and technology?

A likely outcome of our work is a more quantitative prediction of the magnitude of methane flux from the earth to the atmosphere over human (decadal) timescales and geological timescales (10,000 years). These will serve as boundary conditions for atmospheric climate models. In turn, these results may guide policy decisions.

4.7 What dollar amount of the award's budget is being spent in foreign country(ies)?

Zero percent of the award's budget is being spent in foreign countries.

5 CHANGES/PROBLEMS:

5.1 Changes in approach and reasons for change

There are no changes in approach to report for this reporting period.

5.2 Actual or anticipated problems or delays and actions or plans to resolve them

Our biggest challenge is in the experimental realm. It has been more challenging than envisioned to simulate the solidification of hydrate with an advancing gas front. LBNL is also nearly spent out of resources. For this reason we have also built an experimental cell for application at U.T.

5.3 Changes that have a significant impact on expenditures

Dr. Steve Bryant moved to a new academic position effective Sept 1, 2014. As a result he was removed as Co-PI on this project. With approval from sponsor we reallocated unexpended salary plus indirect cost recovery to purchase permanent equipment

5.4 .Significant changes in use or care of human subjects, vertebrate animals, and/or Biohazards

Nothing to report

5.5 Change of primary performance site location from that originally proposed

Nothing to report

6 BUDGETARY INFORMATION:

Budget Period 1													
Baseline Reporting (10/1/12 - 9/30/14)	Q1			Q2			Q3			Q4		
	10/1/12 - 2/15/13			2/16/13-6/30/2013			7/1/2013-11/15/2013			11/16/2013-3/31/2014		
	Q1	Cumulative Total		Q2	Cumulative Total		Q3	Cumulative Total		Q4	Cumulative Total	
Baseline Cost Plan												
Federal Share	$ 136,111.50	$ 136,111.50		$ 175,000.50	$ 311,112.00		$ 175,000.50	$ 486,112.50		$ 175,000.50	$ 661,113.00	
Non-Federal Share	$ 43,568.75	$ 43,568.75		$ 43,568.75	$ 87,137.50		$ 43,568.75	$ 130,706.25		$ 43,568.75	$ 174,275.00	
Total Planned	$ 179,680.25	$ 179,680.25		$ 218,569.25	$ 398,249.50		$ 218,569.25	$ 616,818.75		$ 218,569.25	$ 835,388.00	
Actual Incurred Cost												
Federal Share	$ 45,506.00	$ 45,506.00		$ 67,607.00	$ 113,113.00		$ 258,059.00	$ 371,172.00		$ 137,004.00	$ 508,176.00	
Non-Federal Share	$ -	$ -		$ 81,202.43	$ 81,202.43		$ 26,527.09	$ 107,729.52		$ 10,775.81	$ 118,505.33	
Total Incurred Cost	$ 45,506.00	$ 45,506.00		$ 148,809.43	$ 194,315.43		$ 284,586.09	$ 478,901.52		$ 147,779.81	$ 626,681.33	
Variance												
Federal Share	$ (90,605.50)	$ (90,605.50)		$(107,393.50)	$ (197,999.00)		$ 83,058.50	$ (114,940.50)		$ (37,996.50)	$ (152,937.00)	
Non-Federal Share	$ (43,568.75)	$ (43,568.75)		$ 37,633.68	$ (5,935.07)		$ (17,041.66)	$ (22,976.73)		$ (32,792.94)	$ (55,769.67)	
Total Variances	$(134,174.25)	$(134,174.25)		$ (69,759.82)	$ (203,934.07)		$ 66,016.84	$ (137,917.23)		$ (70,789.44)	$ (208,706.67)	

Budget Period 2												
	Q1			Q2			Q3			Q4		
	4/1/2014-8/15/2014			8/16/2014-12/31/2014			1/1/2015-5/15/2015			5/16/2015-9/30/2015		
	Q1	Cumulative Total		Q2	Cumulative Total		Q3	Cumulative Total		Q4	Cumulative Total	
Baseline Cost Plan												
Federal Share	$ 127,422.00	$ 788,535.00		$ 127,422.00	$ 915,957.00		$ 127,425.00	$ 1,043,382.00		$ 127,425.00	$ 1,170,807.00	
Non-Federal Share	$ 34,048.50	$ 208,323.50		$ 34,048.50	$ 242,372.00		$ 34,048.50	$ 276,420.50		$ 34,048.50	$ 310,469.00	
Total Planned	$ 161,470.50	$ 996,858.50		$ 161,470.50	$ 1,158,329.00		$ 161,473.50	$ 1,319,802.50		$ 161,473.50	$ 1,481,276.00	
Actual Incurred Cost												
Federal Share	$ 202,625.00	$ 710,801.00		$ 38,923.00	$ 749,724.00		$ -	$ 749,724.00		$ -	$ 749,724.00	
Non-Federal Share	$ 27,408.75	$ 145,914.07		$ -	$ 145,914.07		$ -	$ 145,914.07		$ -	$ 145,914.07	
Total Incurred Cost	$ 230,033.75	$ 856,715.07		$ 38,923.00	$ 895,638.07		$ -	$ 895,638.07		$ -	$ 895,638.07	
Variance												
Federal Share	$ 75,203.00	$(152,937.00)		$ (88,499.00)	$ (241,436.00)		$(127,425.00)	$ (368,861.00)		$(127,425.00)	$ (496,286.00)	
Non-Federal Share	$ (6,639.75)	$ (55,769.67)		$ (34,048.50)	$ (89,818.17)		$ (34,048.50)	$ (123,866.67)		$ (34,048.50)	$ (157,915.17)	
Total Variances	$ 68,563.25	$(208,706.67)		$(122,547.50)	$ (331,254.17)		$(161,473.50)	$ (492,727.67)		$(161,473.50)	$ (654,201.17)	

7 Nomenclatures

G	Free gas phase
H	Hydrate phase
L	Liquid phase
u	Pore pressure (MPa)
ρ_{sw}	Seawater Density (g/cm^3)
ρ_{pw}	Pore water density (g/cm^3)
ρ_f	Fluid density (g/cm^3)
ρ_b	Bulk density (g/cm^3)
ρ_m	Grain density (g/cm^3)
Z_{wd}	Water depth (m)
ΔZ	Depth within the GHSZ (m)
Z	GHSZ thickness (m)
g	Gravitational acceleration (m/s^2)
T_f	Formation temperature (ºC)
T_b	Seafloor temperature (ºC)
G_g	Geothermal gradient (ºC/km)
S_h	Hydrate saturation (dimensionless)
S_w	Water saturation (dimensionless)
$C_{in\text{-}situ}$	In-situ salinity (dimensionless)
C_0	Core-derived salinity (dimensionless)
C	Salinity (dimensionless)
N	Saturation exponent (dimensionless)
a	Tortuosity coefficient (dimensionless)
m	Cementation exponent (dimensionless)
n	Porosity (dimensionless)
ρ_w	Fluid resistivity (Ωm)
ρ_t	Formation resistivity (Ωm)
F	Formation factor (dimensionless)

Analytical model

M_m	molar weight of methane (kg mol^{-1})
M_w	molar weight of water (kg mol^{-1})
M_h	molar weight of hydrate (kg mol^{-1})
$m^m_{g,f}$	methane mass in the final gas phase (kg)
$m^m_{h,f}$	methane mass in the final hydrate phase (kg)
$m^m_{w,f}$	methane mass in the final water phase (kg)
$m^m_{g,i}$	methane mass in the initial gas phase (kg)
$m^m_{w,i}$	methane mass in the initial water phase (kg)
N	stoichiometric hydration number (dimensionless)
P_f	final pressure (Pa)
P_i	initial pressure (Pa)
T_f	final temperature (K)
T_i	initial temperature (K)
$S_{g,i}$	initial gas saturation (dimensionless)

$S_{g,f}$	final gas saturation (dimensionless)
$S_{h,f}$	maximum hydrate saturation (dimensionless)
$S_{w,i}$	initial water saturation (dimensionless)
$S_{w,f}$	final water saturation (dimensionless)
V_{tot}	total volume of the sediment (m^3)
$X^m_{w,f}$	final solubility of methane in water (wt.%)
$X^m_{w,i}$	initial solubility of methane in water (wt.%)
$X^s_{w,i}$	initial mass fraction of salt in brine (wt.%)
$X^s_{w,f}$	final mass fraction of salt in brine (wt.%)
$\rho_{w,f}$	initial brine density (kg m^{-3})
$\rho_{w,i}$	final brine density (kg m^{-3})
$\rho_{g,i}$	initial gas density (kg m^{-3})
$\rho_{g,f}$	final gas density (kg m^{-3})
ρ_h	methane hydrate density (kg m^{-3})
ϕ	porosity of the sediment (dimensionless)
Δm	mass of methane gas consumed during hydrate formation (kg)

Numerical model

β	phase
e	energy component
g	gas phase
h	hydrate phase
κ	component
l	liquid phase
m	methane component
s	salt component
v	vapor phase
w	water component
C_R	heat capacity of the solid grain (J kg^{-1} oC^{-1})
D^{κ}_{l0}	molecular diffusion coefficient of component k in free water (m^2 s^{-1})
ϕ	porosity of the sediment (dimensionless)
ϕ_0	porosity in the absence of hydrate (dimensionless)
g	acceleration due to gravity (m s^{-2})
h_β	specific enthalpy of phase β (J kg^{-1})
k	intrinsic permeability (m^2)
k_0	permeability in the absence of hydrate (m^2)
$k_{r\beta}$	relative permeability of phase β (dimensionless)
λ	overall thermal conductivity of porous media (W m^{-1} $^oC^{-1}$)
λ_β	thermal conductivity of phase β (W m^{-1} $^oC^{-1}$)
λ_R	thermal conductivity of grain (W m^{-1} $^oC^{-1}$)
μ_β	viscosity of phase β (Pa s)
P_c	capillary pressure (Pa)
P_{c0}	capillary pressure in the absence of hydrate (Pa)

P_β	β phase pressure (Pa)
q^e	generation rate of energy (J m^{-3} s^{-1})
q^κ	generation rate of component κ (kg m^{-3} s^{-1})
ρ_β	density of phase β (kg m^{-3})
S_β	saturation of phase β (dimensionless)
T	temperature (^{o}C)
t	time (s)
u_β	specific internal energy of phase β (J kg^{-1})
X_β^k	mass fraction of component κ in phase β (dimensionless)

8 References

Archer, D., Buffett, B., and Brovkin, V., 2009, Ocean methane hydrates as a slow tipping point in the global carbon cycle: Proceedings of the National Academy of Sciences, v. 106, no. 49, p. 20596-20601.

Brothers, D. S., Ruppel, C., Kluesner, J. W., ten Brink, U. S., Chaytor, J. D., Hill, J. C., Andrews, B. D., and Flores, C., 2014, Seabed fluid expulsion along the upper slope and outer shelf of the U.S. Atlantic continental margin: Geophysical Research Letters, v. 41, no. 1, p. 2013GL058048.

Dallimore, S., and Collett, T., 2005, Scientific results from the Mallik 2002 gas hydrate production research well program, Mackenzie delta, Northwest Territories, Geological Survey of Canada, Volume Bulletin 601.

Henninges, J., Schrotter, J., Erbas, K., and Huenges, E., 2005, Temperature field of the Mallik gas hydrate occurrence - implication on phase changes and thermal properties, *in* Dallimore, S. R., and Collett, T. S., eds., Scientific Results from the Mallik 2002 Gas Hydrate Production Research Well Program, Mackenzie Delta, Northwest Territories, Canada, Volume Bulletin 585, Geological Survey of Canada, p. 11.

Majorowicz, J., Osadetz, K., and Safanda, J., 2012, Gas Hydrate Formation and Dissipation Histories in the Northern Margin of Canada: Beaufort-Mackenzie and the Sverdrup Basins: Journal of Geological Research, v. 2012.

Reagan, M. T., and Moridis, G. J., 2009, Large-scale simulation of methane hydrate dissociation along the West Spitsbergen Margin: Geophysical Research Letters, v. 36, no. 23, p. L23612.

Skarke, A., Ruppel, C., Kodis, M., Brothers, D., and Lobecker, E., 2014, Widespread methane leakage from the sea floor on the northern US Atlantic margin: Nature Geosci, v. 7, no. 9, p. 657-661.

Taylor, A. E., Dallimore, S. R., Hyndman, R. D., and Wright, F., 2005, Comparing the sensitivity of terrestrial and marine gas hydrates to climate warming at the end of the last ice age.: Geological Survey of Canada Bulletin.

National Energy Technology Laboratory

626 Cochrans Mill Road
P.O. Box 10940
Pittsburgh, PA 15236-0940

3610 Collins Ferry Road
P.O. Box 880
Morgantown, WV 26507-0880

13131 Dairy Ashford Road, Suite 225
Sugar Land, TX 77478

1450 Queen Avenue SW
Albany, OR 97321-2198

Arctic Energy Office
420 L Street, Suite 305
Anchorage, AK 99501

Visit the NETL website at:
www.netl.doe.gov

Customer Service Line:
1-800-553-7681